Spin-dependent surface barrier from very-low-energy electron diffraction fine structures: A feasibility study

U. Burgbacher,[1] J. Braun,[2] A. K. Brüning,[1] A. B. Schmidt,[1] and M. Donath[1,*]

[1]*Physikalisches Institut, Westfälische Wilhelms-Universität Münster, Wilhelm-Klemm-Straße 10, 48149 Münster, Germany*

[2]*Department Chemie, Ludwig-Maximilians-Universität München, Butenandtstraße 5-13, 81377 München, Germany*

(Received 8 February 2013; revised manuscript received 4 March 2013; published 8 May 2013)

The surface barrier is a key issue for understanding and describing the results of surface-sensitive electron spectroscopies, such as photoemission and inverse photoemission. We present a feasibility study showing that the shape of the surface barrier can be derived from very-low-energy electron diffraction (VLEED) fine-structure measurements. In particular, we focus on the spin dependence of the barrier probed by a spin-polarized experiment. We show model calculations of spin-dependent fine structures for specific ferromagnetic surfaces, where spin-dependent barrier models were successfully employed to describe spectroscopic results. We come to the conclusion that spin-polarized VLEED experiments with state-of-the-art energy and angular resolution are able to reveal details of the spin-dependent shape of the surface barrier.

DOI: 10.1103/PhysRevB.87.195411 PACS number(s): 73.20.At, 75.70.−i, 68.49.Jk, 75.25.−j

I. INTRODUCTION

Very-low-energy electron diffraction (VLEED) is the most important experimental tool for analyzing the shape of the surface (-potential) barrier at single-crystal surfaces. Fine structures appear in intensity vs energy curves $I(E)$ of elastically reflected very-low-energy electrons. The energy position and the shape of these fine structures are directly sensitive to the surface-barrier shape. Thus, measuring the fine structure provides experimental access to the surface barrier.[1,2]

The potential in front of a metal surface, referred to as the surface barrier, comprises the Coulomb-like image potential on the vacuum side far from the crystal surface and the transition region between the image potential and the inner potential of the crystal. To ensure a smooth transition between the two different potentials, various barrier models have been proposed.[3–5] The width of the surface barrier is of the order of the lattice constant of the crystal. Because of its localization directly at the surface, the surface barrier influences the energetics and dispersion $E(k_{\parallel})$ of surface states. Additionally, it determines electron transfer processes through conductive surfaces for electrons with kinetic energies below 50 eV. Therefore, the surface barrier is essential for the interpretation of data from electron spectroscopies such as (inverse) photoemission and low-energy electron diffraction (LEED). Recently, the interest in a detailed understanding of the spin-dependent surface electronic structure has strongly increased due to the interesting spin-orbit-induced phenomena appearing in Rashba systems[6–8] and topological insulators.[9–15]

In 1964, McRae and Caldwell were the first to observe a fine structure in VLEED $I(E)$ curves on LiF(100).[16] Since then, a variety of surfaces has been studied experimentally by means of VLEED.[17–22] Many of these experiments were combined with calculations of VLEED $I(E)$ curves to determine a surface-barrier shape for the surfaces under consideration.[3–5,21] In the 1970s, the electron spin became an important quantity in LEED experiments on high-Z materials. In accordance with theoretical predictions, the elastic scattering amplitude of electrons at W(001) turned out to be spin dependent due to spin-orbit coupling. This led to the development of a spin-polarization detector based on spin-polarized low-energy electron diffraction (SPLEED).[23–25] In spin-polarized VLEED on differently oriented tungsten single crystals, a spin dependence of the fine structure was observed. This, however, has been ascribed primarily to spin-dependent crystal scattering rather than to a spin-dependent surface barrier.[26–28]

On a ferromagnetic surface, additionally a spin-dependent surface barrier is expected due to exchange interaction. Inverse-photoemission studies on image-potential surface states on Fe(110) suggest a spin dependence of the surface barrier.[29] It turned out that two qualitatively different shapes for the spin-dependent surface barrier can be used to explain the experimental data.[30,31] To the best of our knowledge, no spin-polarized measurements of the VLEED fine structure at a ferromagnetic system can be found in literature. Nevertheless, a new type of spin-polarization detector has been developed, based on electron scattering from ferromagnetic Fe(001) films.[32,33] This detector benefits from the large scattering amplitude of very-low-energy electrons combined with a large spin asymmetry.

The aim of this paper is to provide a feasibility study of the possibility of determining the spin-dependent shape of the surface barrier with spin-polarized very-low-energy electron diffraction. The question is whether a state-of-the-art spin-polarized VLEED experiment is capable of resolving the potentially small differences in a spin-dependent surface barrier. To anticipate the answer: Such a distinction turns out to be possible.

We start with a tutorial-like review of some of the experimental and theoretical VLEED studies found in the literature over the last five decades. Section II introduces the concept of the surface barrier. In Sec. III we describe how the shape of the surface barrier can be derived from VLEED $I(E)$ data. In Sec. IV experimental aspects are reviewed, in particular how the experimental resolution influences VLEED spectra. Section V summarizes the details of our calculations. In Sec. VI we present VLEED $I(V)$ curves calculated for different surface barriers to show how the surface-barrier shape affects the VLEED fine structure in general. Finally, we predict VLEED fine structures for Co(0001) and Fe(110)

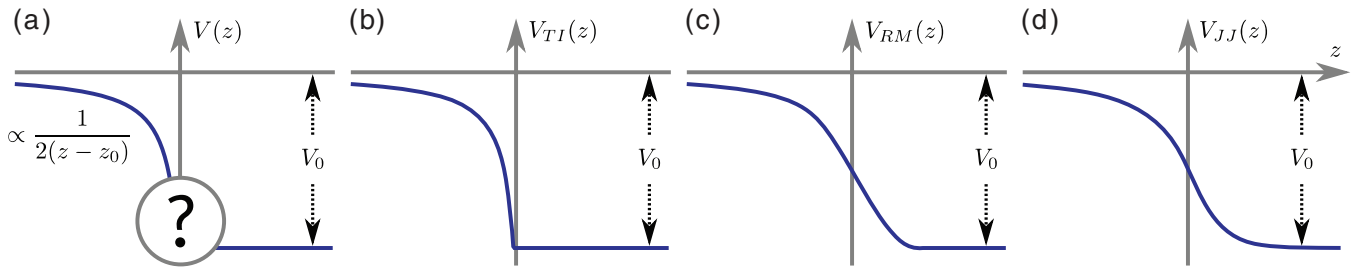

FIG. 1. (Color online) Surface-barrier models. (a) The region of interest is the transition between the image potential on the vacuum side and the constant inner potential V_0 within the metal. (b) The simplest transition is described by the "truncated" image potential V_{TI}. (c),(d) Two more realistic barrier models are the Rundgren-Malmström barrier V_{RM} and the Jennings-Jones barrier V_{JJ}.

based on the spin-dependent surface-barrier models available in the literature.[30,31,34]

II. SURFACE BARRIER

The general shape of the surface barrier can be derived from two basic assumptions: From classical electrostatics it is known that the shape of the potential $V(z)$ of a charged particle at a distance z in front of a metallic surface is Coulomb-like:[35]

$$V(z) = \frac{1}{2(z - z_0)}, \quad z < z_0.$$

The classically defined metal-vacuum interface is located at z_0, which is also referred to as the "classical image plane." The classical description has proven to be correct for the region far outside the conductor, i.e., where $z \ll z_0$, but the potential diverges upon approaching z_0. Inside a free-electron metal, a constant "inner" potential V_0 is assumed. The transition region between the Coulomb-like image potential far outside the conductor and the constant inner potential inside the conductor is a matter of debate [cf. Fig. 1(a)]. The determination of the surface-barrier shape can basically be reduced to the following problems:

(a) Where is the classical image plane z_0 located relative to the topmost atomic layer?

(b) What is the exact shape of the transition region?

The simplest model for a surface barrier is a truncated image potential V_{TI} [Fig. 1(b)]. The image potential is "cut" by the constant inner potential, resulting in a sharp kink at the transition. There is little physical justification for this model besides its simplicity. More sophisticated approaches derive the transition between the two potentials from a quantum mechanical treatment. A detailed review on this topic is given by Jennings and Jones.[36]

Several authors have derived analytical models of the surface-potential barrier from *ab initio* calculations (see, e.g., Refs. 36 and 37) in order to incorporate the surface barrier into the calculation schemes for LEED or photoemission intensities. Which barrier model is most suitable to describe a certain metal surface has to be decided usually on a case-by-case basis. Widespread models are the Rundgren-Malmström barrier[3] and the Jennings-Jones barrier.[4]

The Rundgren-Malmström barrier,[38] shown in Fig. 1(c), connects the asymptotic regime $z \leqslant z_1$ to the bulk muffin-tin zero V_0 by a third-order polynomial in z, spanning the range $z_1 < z < z_2$. The zero of the z scale lies in the outermost layer of atoms. For the real parts of $V_{\mathrm{RM}}(z)$ we have

$$V_{\mathrm{RM}}(z) = \begin{cases} \frac{1}{2}(z - z_0)^{-1}, & z \leqslant z_1 < z_0, \\ s_0 + s_1(z - z_1) + s_2(z - z_1)^2 & \\ \quad + s_3(z - z_1)^3, & z_1 < z < z_2, \\ V_0, & z \geqslant z_2. \end{cases} \tag{1}$$

The imaginary parts of the barrier potential have been set to zero, avoiding the introduction of additional parameters. The polynomial coefficients s_0, s_1, s_2, and s_3 are fixed through the requirement of continuity and differentiability for $V_{\mathrm{RM}}(z)$.

The Jennings-Jones barrier[4] is given by

$$V_{\mathrm{JJ}}(z) = \begin{cases} \frac{1}{2(z - z_0)}(1 - e^{\lambda(z - z_0)}), & z \leqslant z_0, \\ \frac{-V_0}{A \exp[-B(z - z_0)] + 1}, & z > z_0. \end{cases}$$

A and B are determined by matching $V_{\mathrm{JJ}}(z)$ and its derivative at z_0.

These model barriers imply that the surface barrier is one dimensional. This is obviously a simplification since the charge density of a real crystal surface is corrugated lateral to the surface. Tamura and Feder[39] showed that barrier corrugation may have an influence on VLEED spectra of W(001) at energies below 12 eV. They compared experimental data with calculations based on one- and three-dimensional barrier models.

The shape of the surface barrier results from a rearrangement of electrons near the Fermi level. Since the density of states in ferromagnetic surfaces is spin dependent, impinging electrons with different spin directions interact differently with the electronic system of the crystal due to exchange interaction. This effect was predicted for a Fe(110) surface by Nekovee *et al.*[30] and supported by inverse photoemission experiments.[29,31]

III. VLEED FINE STRUCTURE

Experimentally, the properties of the surface barrier can be studied by examining the scattering characteristics of the barrier. Typically, a collimated, monoenergetic electron beam is directed onto the crystal surface. The electrons are partly transmitted into the crystal and partly reflected back into the vacuum. The amount I of very-low-energy electrons (0–30 eV) specularly and elastically reflected contains valuable information about the shape of the surface barrier.[40] Hence, the observable of a VLEED experiment is the intensity $I(E, \Theta, \Phi)$. E is the kinetic energy of the electrons, and Θ and Φ are

the angles of incidence relative to the surface normal and relative to an in-plane high-symmetry direction of the surface, respectively. In a spin-polarized VLEED experiment, there are two observables $I^{\uparrow}(E,\Theta,\Phi)$ and $I^{\downarrow}(E,\Theta,\Phi)$ for incoming electrons with spin magnetic moment parallel or antiparallel to a given quantization axis. In a ferromagnet typically the magnetization direction is chosen. Usually, Θ and Φ are held constant while varying the energy E of the incoming (and reflected) electrons.

Due to scattering at the surface barrier, features in these $I(E)$ profiles arise which consist of oscillations that converge toward certain energies. The main properties of these so-called fine structures are as follows:[41]

(a) The associated peaks are at least an order of magnitude narrower in energy than the prominent Bragg peaks. They are clearly recognizable at very low energies and are no longer resolved as the energy increases.

(b) The series of peaks converges from lower energies toward the emergence threshold $E_{\mathbf{g}}$ of a new diffracted beam. The peak positions E_n and widths Γ_n are approximately given by

$$E_n = E_{\mathbf{g}} - 1/(n-a)^2, \quad n = 1,2,3,\ldots,$$
$$\Gamma_n = 1/(n-b)^3,$$

with a and b as parameters. This Rydberg-like series is attributed to the Coulomb-like part of the surface barrier.

Since the incoming electrons are scattered not only by the surface barrier but also by the crystal itself, it is not possible to examine the properties of the barrier and the crystal separately. Instead, both processes have to be incorporated into a model that allows the scattering of an electron at a metal surface to be described. The following sections give a description of how the Rydberg series evolves from the combined scattering at the surface barrier and at the crystal.

A. Crystal scattering

Crystal scattering of low-energy electrons is a research area which has been widely studied (for reviews see, e.g., Refs. 24, and 42–45). Here, we want to recall some results of the kinematic LEED theory that are important for understanding the VLEED fine structure: A plane wave (with wave vector $\mathbf{k}_0$) impinges on the two-dimensional surface mesh and is scattered by each ion core of the crystal surface. The scattered waves interfere to give a set of diffracted beams (i.e., plane waves). Each of these beams is described by a single wave vector $\mathbf{k}$. Parallel to the surface, the difference in momentum of the diffracted beams and the incident beam can be described by the Laue condition

$$\mathbf{k}_{\parallel} - \mathbf{k}_{0\parallel} = \Delta\mathbf{k}_{\parallel} = \mathbf{g}, \tag{2}$$

where $\mathbf{g}$ is a reciprocal lattice vector of the two-dimensional surface mesh. Since the diffraction process is elastic, conservation of energy applies and with Eq. (2) the perpendicular component $\mathbf{k}_{\perp}$ of $\mathbf{k}$ is determined by

$$E = \tfrac{1}{2}(|\mathbf{k}_{0\parallel}|^2 + |\mathbf{k}_{0\perp}|^2) = \tfrac{1}{2}(|\mathbf{k}_{\parallel}|^2 + |\mathbf{k}_{\perp}|^2). \tag{3}$$

After the exchange of a reciprocal lattice vector, we have

$$E = \tfrac{1}{2}(|\mathbf{k}_{0\parallel} + \mathbf{g}|^2 + |\mathbf{k}_{\perp}|^2). \tag{4}$$

A beam can propagate into the vacuum only if the momentum perpendicular to the surface is greater than zero. Equation (4) determines a threshold energy for the emergence of a new beam with the corresponding reciprocal lattice vector $\mathbf{g}$:

$$E_{\mathbf{g}}(|\mathbf{k}_{\perp}| = 0) = \tfrac{1}{2}|\mathbf{k}_{0\parallel} + \mathbf{g}|^2. \tag{5}$$

This threshold energy (or emergence threshold) is important because the VLEED fine structure always appears as a Rydberg-like series converging towards this threshold. A beam with energy just below this threshold is called a preemergent beam.

Kinematic LEED theory gives some basic insights into the principles of electron diffraction. It cannot, however, predict the shape of $I(E)$ profiles because many features of $I(E)$ curves are induced by multiple scattering of the incoming plane waves at atomic layers. Dynamical LEED theories address this problem by transforming the incident plane-wave amplitudes into the amplitudes (and thus the intensities) of the emerging diffracted beams. This transformation can be described by the bulk-reflection matrix $\mathbf{R}$. Hence, the problem lies in the determination of $\mathbf{R}$. Calculation schemes for $\mathbf{R}$ can be found in Ref. 42 or 24 and references therein.

Due to spin-orbit coupling, electron scattering by high-Z atoms is spin dependent. The spin dependence of electron scattering at ion cores is low for LEED energies. Due to interference effects caused by multiple scattering, however, the whole scattering process can be highly spin dependent. This is the basis for the SPLEED spin-polarization detector.[23] If a ferromagnetic surface is involved, an additional spin dependence is caused by exchange interaction,[24] which is exploited in recently developed detectors.[32,33,46]

B. Barrier scattering

If one describes the barrier as a one-dimensional potential, the electronic wave can be reflected and/or transmitted by the barrier, but the magnitude of the $\mathbf{k}_{\parallel}$ vector never changes. One-dimensional scattering of an incoming plane wave is usually described by four complex scattering coefficients (or "scattering amplitudes") r^{+-}, r^{-+}, t^{++}, and t^{--}. The coefficients r^{+-} and r^{-+} transform incident plane-wave amplitudes into the amplitudes of reflected beams. t^{++} and t^{--} are used to describe the transmission of beams. With these four coefficients determined, the scattering problem is solved. The scattering coefficients of most barrier models (such as the Rundgren-Malmström, the Jennings-Jones and the truncated image potential models) can only be calculated numerically. A detailed review of how this can be done is given in Ref. 41.

C. Combining the scattering processes

The next step now is to answer the question of how crystal and barrier scattering can lead to a fine structure in a VLEED $I(E)$ spectrum. Experimentally (e.g., Ref. 22), the reflected intensity of a specularly and elastically reflected electron beam shows fine structures that consist of a series of Rydberg-like peaks. The Rydberg-like behavior of the fine structure implies that it is caused by the Coulomb-like tail of the surface barrier. However, calculations of the reflected intensity by a Rundgren-Malmström[3] or Jennings-Jones[41]

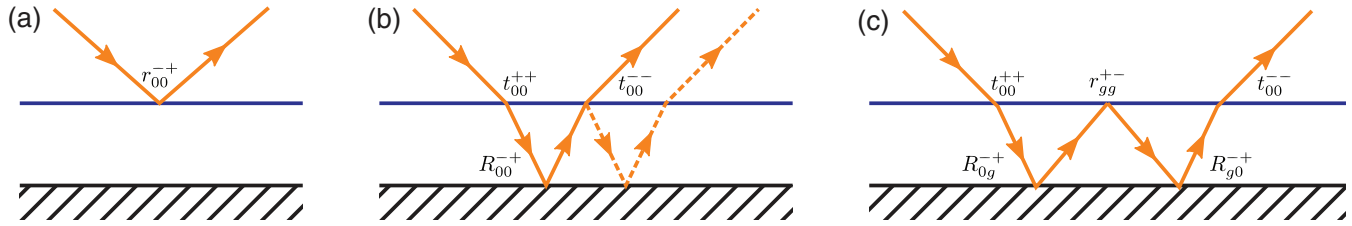

FIG. 2. (Color online) Reflection and diffraction at the crystal and the barrier. (a) Direct reflection at the barrier. (b) Direct reflection at the crystal surface (with backreflection at the barrier represented by the dashed lines). (c) Indirect reflection involving diffraction at the crystal surface.

barrier alone do not show oscillating behavior as long as crystal scattering is neglected. On the other hand, LEED calculations which disregard the surface barrier exhibit no fine structures.[42] Consequently, the fine structure must be caused by interference between the crystal and the barrier scattering process.

Several elastic processes contribute to the specularly backscattered intensity (see Fig. 2):[41]

(1) The incident electron beam is reflected directly at the barrier [Fig. 2(a)].

(2) The incident electron beam is transmitted through the barrier, then reflected at the crystal, and further on transmitted through the barrier into the vacuum [Fig. 2(b)].

(3) Additionally, after reflection at the crystal, the beam is reflected back at the barrier. This process can occur repeatedly until the electron is transmitted into the vacuum again [Fig. 2(b), dashed line].

(4) Since the crystal surface exhibits a periodic structure, the $\mathbf{k}_\parallel$ component of the incident beam may change by the amount of a reciprocal lattice vector $\mathbf{g}$ of the surface mesh when the beam is reflected at the crystal. Afterwards, all the above-mentioned processes can occur. Yet the change of $\mathbf{k}_\parallel$ removes the beam from the specularly reflected intensity. Only beams that are diffracted back into the specular direction (i.e., by changing their wave vector $\mathbf{k}_\parallel$ by $-\mathbf{g}$) can contribute to the intensity of the specular beam [Fig. 2(c)].

Summing up all these possible processes yields the total amplitude A_{00} of the specularly reflected beam (where R describes the bulk reflection, and the subscripts indicate the value of $k_\parallel$ relative to $k_{0\parallel}$):

$$A_{00} = r_{00}^{-+} + t_{00}^{--} R_{00}^{-+} t_{00}^{++} + t_{00}^{--} R_{00}^{-+} r_{00}^{+-} R_{00}^{-+} t_{00}^{++} + t_{00}^{--} R_{0g}^{-+} r_{gg}^{+-} R_{g0}^{-+} t_{00}^{++} + \cdots. \quad (6)$$

Le Bosse *et al.*[47] determined which physical processes mainly contribute to the fine structures. The primary cause of a VLEED fine structure is a two-beam interference of the primary electron beam with a diffracted, preemergent beam. Another, but less important, contribution comes from the presence of surface-state resonances. Both processes will be described in the next paragraphs.

1. Two-beam interference

The main process which leads to fine structures is comparable with two-beam interference from a parallel plate as is known from optics. Interference between direct reflection at the crystal surface [as shown in Fig. 2(b)] and indirect reflection involving diffraction [and back diffraction into the specular direction as shown in Fig. 2(c)] cause a Rydberg-like fine structure in VLEED spectra.

Qualitatively, the incident electron wave loses momentum perpendicular to the surface during the diffraction process. Now the electron may have insufficient energy to overcome the barrier and will be reflected back towards the crystal. Here, it may be diffracted back into the specular direction and thus regain the energy needed to propagate into the vacuum.

Since the fine structure appears at preemergence conditions, the energy E of the primary (incident) beam must be below the grazing-emergence energy $E_\mathbf{g}$ [cf. Eq. (5)]. This is equivalent to $e_\perp < 0$ if $e_\perp$ is the energy characterizing the perpendicular momentum of the diffracted beam (as illustrated in Fig. 3).

Now incoming plane waves with different primary energies are considered. After being diffracted, their energies $e_\perp$ will also be different, even if their propagation vectors have changed by the same reciprocal lattice vector $\mathbf{g}$. As $e_\perp$ approaches the vacuum level, the Coulomb-like tail of the image potential becomes increasingly shallow. Thus, waves with only a small difference in $e_\perp$ have to travel distances which differ by increasingly large amounts Δz before they are reflected at the barrier (cf. Fig. 4).

Two-beam interference is described by taking into account only the first three members of the series given in Eq. (6). High intensity in the VLEED fine structure appears for constructive interference between the processes (a), (b), and (c) in Fig. 2. Due to the long Coulomb-like tail in the surface potential, the interval between energies which meet the condition for constructive interference decreases as $e_\perp$ approaches the vacuum level. This is the cause of the Rydberg series.

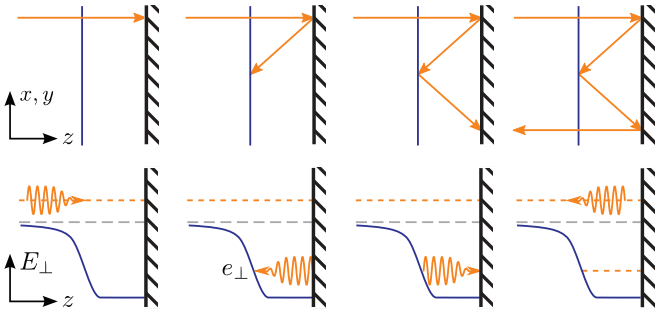

FIG. 3. (Color online) Schematic representation of the parallel component of the wave vector during the diffraction process as well as the energy corresponding to the perpendicular component of the wave vector.

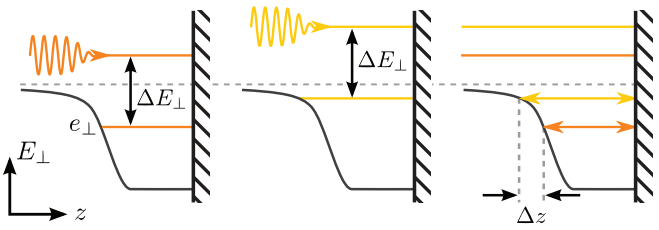

FIG. 4. (Color online) Two beams with different primary energies $E_\perp$ (left and middle) experience a difference Δz in the distance the diffracted beams have to travel (right) before they are reflected at the barrier.

2. *Surface-state resonances*

In the presence of conditions that support the existence of a bound surface state, the electron may become trapped between the crystal and the barrier.[48] Now, instead of only one internal reflection at the barrier, the diffracted wave can be reflected an infinite number of times at the barrier.

The resonant scattering can be qualitatively described as follows: As the electron beam impinges on the crystal, it is diffracted so that the propagation vector is changed by a reciprocal lattice vector **g**. The energy $e_\perp$ is now below the vacuum level. If the conditions for a bound surface state are met at $e_\perp$, the electron occupies this state. If the electron does not decay into the crystal, the electron can be diffracted back into the specular channel. This scattering process, which can occur only at the energies of bound states, yields maxima in the reflectivity.[1]

The two-beam interference mechanism is more universal than the resonance scattering processes because it does not rely on the existence of a bound surface state. Therefore, the condition for the two-beam interference is weaker than the resonance condition and it is usually the primary cause of VLEED fine structures.[47] Consequently, VLEED is more versatile for examining the surface barrier than other electron spectroscopies, which rely on the existence of bound surface states.

D. Fine-structure calculations for different surface-barrier models

Figure 5 shows fine structures that have been calculated using the two-beam interference approximation for three different barrier models. The scattering amplitude R^{-+} of the crystal is kept constant in these model calculations. The parameters of the Rundgren-Malmström and the Jennings-Jones barriers are chosen such that the fine structure is influenced only by the intrinsic shape differences (which is not possible for the "truncated" image potential). The largest differences in peak position and shape occur for the first fine-structure maxima and minima. Since all barrier models exhibit the Coulomb-like image-potential tail for $z \to -\infty$, the shape of the barrier cannot be distinguished by analyzing the Rydberg peaks of higher order. Therefore, from an experimental point of view, it is more important to resolve the first (lowest-energy) peaks than the high-order fringes.[49,50]

IV. EXPERIMENTAL ACCESS

In a VLEED experiment, electrons with variable kinetic energy E from 0 to 50 eV are directed onto a sample under

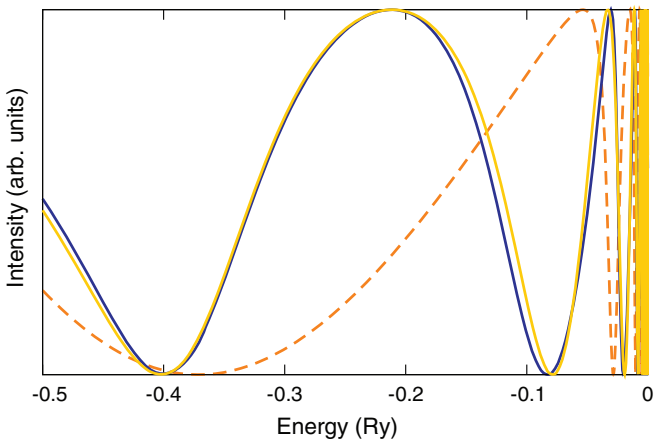

FIG. 5. (Color online) Model calculations of VLEED fine structures within the two-beam approximation for three different barriers: Rundgren-Malmström barrier (orange/grey), Jennings-Jones barrier (blue/black) and the truncated image potential (dashed).

defined angles of incidence Θ and azimuth angles Φ (see the inset in Fig. 6). The elastically and specularly reflected electron intensity I is measured as a function of energy E in $I(E)$ curves. In the energy range under consideration, the VLEED $I(E)$ curves are explicitly affected by the surface barrier. VLEED measurements have to be performed under ultrahigh-vacuum conditions on well-prepared, atomically flat single-crystal surfaces. The overall experimental resolution, determined by the electron source and detector, limits the number of Rydberg peaks which can be resolved in a VLEED experiment. Fortunately, as mentioned above, the barrier shape mainly affects the low-order members. An ideal experiment allows for a large variation of experimental parameters, i.e., of electron energy E and angle of incidence Θ and azimuth

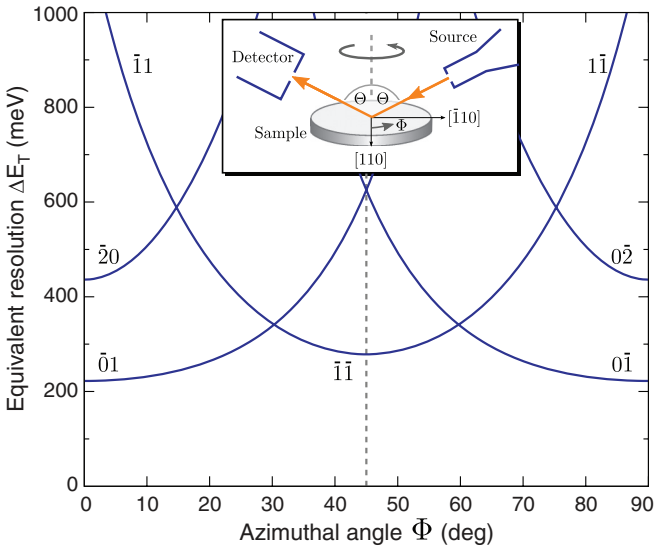

FIG. 6. (Color online) Azimuthal dependence of the equivalent resolution for different fine structures of the Cu(001) surface at a fixed angle of incidence $\Theta = 63^\circ$. Here, an energy distribution of the incoming electron beam of $\Delta E = 200$ meV and an angular distribution of $\Delta\Theta = \Delta\Phi = 1.8^\circ$ were assumed.

angle Φ simultaneously.[49] In this way, the surface barrier is "scanned."

An example for a VLEED apparatus is described by Thurgate and Hitchen.[51] With an energy resolution of $\Delta E = 140$ meV full width at half maximum and an angular resolution of $\pm 0.5^\circ$, they observe up to three fine-structure members in $I(E)$ curves at the Cu(001) surface for specific electron incidence conditions E, Θ, and Φ.[52] Another example for a VLEED apparatus is reported by Dietz *et al.*[21] The quoted resolution is 20 meV and 0.5° full width at half maximum. For a single set of electron incidence parameters chosen in this experiment, there are three members of the Cu(001) series resolved and a fourth one is visible as a shoulder in the presented $I(E)$ curve. Here, however, Θ and Φ could not be varied.

Spin-polarized electrons promise access to a possible spin dependence of the surface barrier, caused either by exchange interaction at ferromagnetic surfaces or by spin-orbit interaction at surfaces of high-Z materials (or combinations thereof). To be able to separate magnetic and nonmagnetic contributions to the spin dependence of the fine structure, the respective polarization direction of the electrons has to be taken into account for the experimental geometry.[53] Examples for VLEED experiments on systems with strong spin-orbit coupling with a spin-polarized electron source or a spin-polarization detector are given by Pierce *et al.*[26] and Samarin *et al.*,[28] respectively. A spin-polarized VLEED experiment on a ferromagnetic system has, to our knowledge, not been published so far.

A. Equivalent resolution

In any experiment, the measured spectra are broadened by the limited resolution in the excitation as well as in the detection channel. In a typical photoemission experiment, for example, the spectrum observed experimentally is broadened by the apparatus function representing a combination of the energetic width of the exciting light with the energy and angular resolution of the detector. In a VLEED experiment, the energy distribution ΔE and the angular distributions $\Delta\Theta$ and $\Delta\Phi$ of the incoming electron beam as well as the detector resolution ΔE_D have to be accounted for. Due to the diffraction process, the normal kinetic energy $e_\perp$ is a function of E, Θ, and Φ [cf. Eq. (4)]. Consequently, ΔE, $\Delta\Theta$, and $\Delta\Phi$ contribute to the broadening $\Delta e_\perp$ of the preemergent beam, their individual "share" depending on the incidence conditions E, Θ, and Φ, as well as on the reciprocal lattice vector exchanged in the diffraction process. The broadening of the observable elastically reflected electron intensity (subject to interference processes) is called "total equivalent resolution" ΔE_T. Convoluted with the detector resolution ΔE_D, this gives the overall broadening of the VLEED spectra measured with a particular setup.

For Gaussian distributions of E, Θ, and Φ with full widths at half maximum ΔE, $\Delta\Theta$, and $\Delta\Phi$, and close to the emergence threshold, ΔE_T can be calculated analytically. A detailed derivation of all relevant formulas can be found in Ref. 50. There, the authors also conclude that the angular resolution of a VLEED setup, rather than the energy resolution, usually plays the more crucial role in whether a fine structure can be resolved. Especially for high energies, the total equivalent resolution is dominated by the angular distribution of the incident electron beam. Incidentally, with an equivalent resolution ΔE_T of a certain minimum value, a detector resolution ΔE_D much better than that is not necessary to improve the experimental resolution significantly.

Calculated fine structures have to be separately convoluted with the corresponding equivalent resolution, since the equivalent resolution depends strongly on the angles of incidence and the reciprocal lattice vector. This is illustrated in Fig. 6, which shows the azimuthal dependence of the equivalent resolution for different fine structures of the Cu(001) surface.

For a certain fine structure at defined angles Θ and Φ, it can be seen from contour plots of $\Delta E_T(\Delta E, \Delta\varphi)$ (with $\Delta\varphi = \Delta\Theta = \Delta\Phi$), whether the energy or the angular resolution is the limiting factor for resolving a particular fine structure. An example is shown on the left-hand side of Fig. 7 for the $\bar{1}\bar{1}$ fine structure of Cu(001) at $\Theta = 63^\circ$ and $\Phi = 45^\circ$, i.e., the fine structure resulting from the exchange of the reciprocal lattice vector $\mathbf{g} = (\bar{1}, \bar{1})$. From the concentric shape of the isolines,

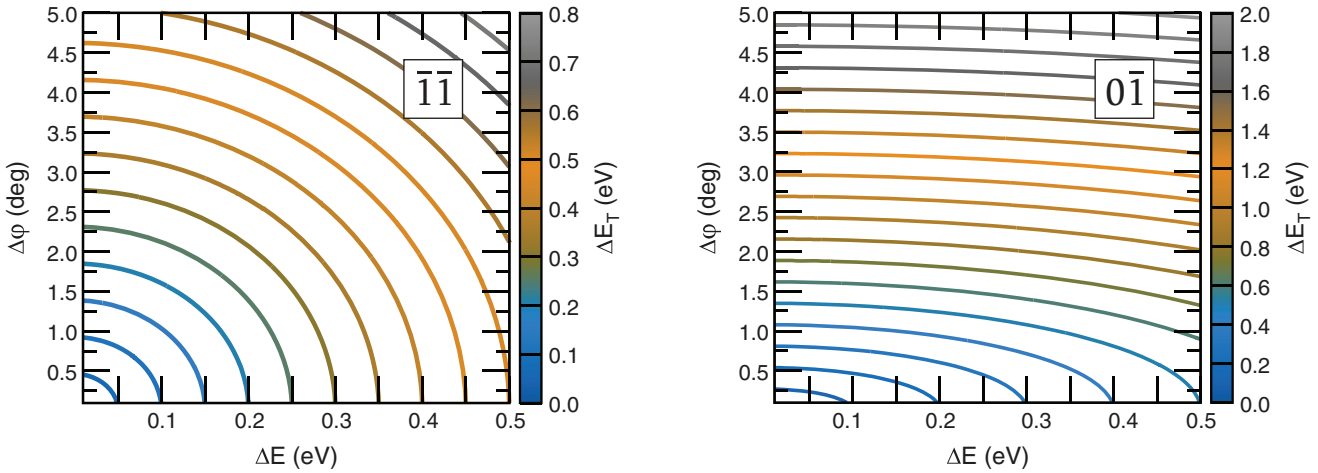

FIG. 7. (Color) Dependence of the equivalent resolution on $\Delta\varphi$ and ΔE for different fine structures of the Cu(001) surface at a fixed angle of incidence $\Theta = 63^\circ$ and a fixed azimuthal angle $\Phi = 45^\circ$. Left: $\bar{1}\bar{1}$ fine structure. Right: $0\bar{1}$ fine structure. Note the different scales of the total equivalent resolution.

it can be derived that the energy and angular resolution are equally important for this structure. For example, an angular resolution of $\Delta\varphi = 4^\circ$ and and energy resolution of $\Delta E = 0.1$ eV gives the same equivalent resolution as an experiment with $\Delta\varphi = 0.5^\circ$ and $\Delta E = 0.45$ eV. However, looking at the right-hand side of Fig. 7, which shows ΔE_T at the same angles for the $0\bar{1}$ fine structure, it becomes clear that the resolution is dominated by the angular resolution.

V. DETAILS OF THE CALCULATION

Our spin-polarized VLEED calculations are based on the layer Korringa-Kohn-Rostoker formulation introduced first by Pendry[42] and later on generalized to the relativistic case by Feder.[24] For such a calculation one needs as an input quantity the so-called single-site scattering matrix, which describes the scattering properties of a single ion-core potential. The scattering matrix is usually obtained from a self-consistent electronic structure calculation of the corresponding material. We used the fully relativistic Korringa-Kohn-Rostoker multiple scattering theory[54,55] to obtain these matrices for fcc Cu, hcp Co, and bcc Fe bulk materials.

Knowing the scattering properties of a single cell potential, one can define in a second step the scattering matrix for a certain layer of the semi-infinite half space. With this matrix we account for all intralayer-type multiple-scattering events. The interlayer multiple scattering is then accounted for by means of layer-doubling techniques.[42] Hereafter, we are left with the bulk-reflection matrix **R**, which gives the scattering properties of a semi-infinite stack of layers. Finally, it remains a simple task to include the very surface described by a barrier potential in the multiple-scattering formalism as an additional layer.

Here, we employ the Rundgren-Malmström barrier[38] as introduced in Eq. (1) of Sec. II. All barrier parameters are taken from the literature, where they have been successfully used to describe surface states and their dispersion. For the ferromagnetic materials, the surface barrier is expected to be spin dependent. Consequently, all parameters are spin dependent, with $\uparrow$ ($\downarrow$) denoting the majority-spin (minority-spin) component.

(a) Cu(001) (Ref. 56): $z_0 = -1.93$ a.u., $z_1 = -3.97$ a.u., and $z_2 = -0.52$ a.u.

(b) Co(0001) (Ref. 34): $z_0^{\uparrow(\downarrow)} = -2.0(-1.7)$ a.u., $z_1^{\uparrow(\downarrow)} = -3.0\ (-3.0)$ a.u., and $z_2^{\uparrow(\downarrow)} = -0.9\ (-0.9)$ a.u.

(c) Fe(110) (Ref. 31): $z_0^{\uparrow(\downarrow)} = -2.0\ (-2.15)$ a.u., $z_1^{\uparrow(\downarrow)} = -3.7\ (-3.85)$ a.u., and $z_2^{\uparrow(\downarrow)} = -0.3(-0.45)$ a.u.

(d) Fe(110) (parametrization of the surface barrier used in Ref. 30): $z_0^{\uparrow(\downarrow)} = -1.6\ (-1.88)$ a.u., $z_1^{\uparrow(\downarrow)} = -1.76\ (-3.92)$ a.u., and $z_2^{\uparrow(\downarrow)} = -0.33\ (-0.42)$ a.u.

The imaginary part of the inner potential was taken constant with $V_{0i} = 0.1$ eV for all three materials.

VI. IMPLICATIONS

A. Sensitivity to different barrier shapes

In this section we will investigate the sensitivity of the VLEED fine structure to changes in the surface-barrier shape, in particular, what experimental resolution is necessary to detect such changes. As an example, we compare calculated profiles of the $\bar{1}\bar{1}$ fine structure of Cu(001) for the Rundgren-Malmström barrier with different parameters. We calculated $I(E)$ curves for six different positions of the image plane z_0 around the literature value given above, while keeping the parameters z_1 and z_2 constant. We move z_0 successively towards the crystal surface. The change in z_0 between two consecutive barriers is 0.05 Å. This leads from a round concave shape to an almost linear transition into the inner potential. A similar change in the shape of the barrier can be achieved by changing the other parameters. The left-hand side of Fig. 8 shows the results of the calculation: The positions, shapes, and intensities of different fine-structure maxima and minima change. The position of the first fine-structure peak appears to be most sensitive. It changes by 100–150 meV for a shift of the image plane by 0.05 Å.

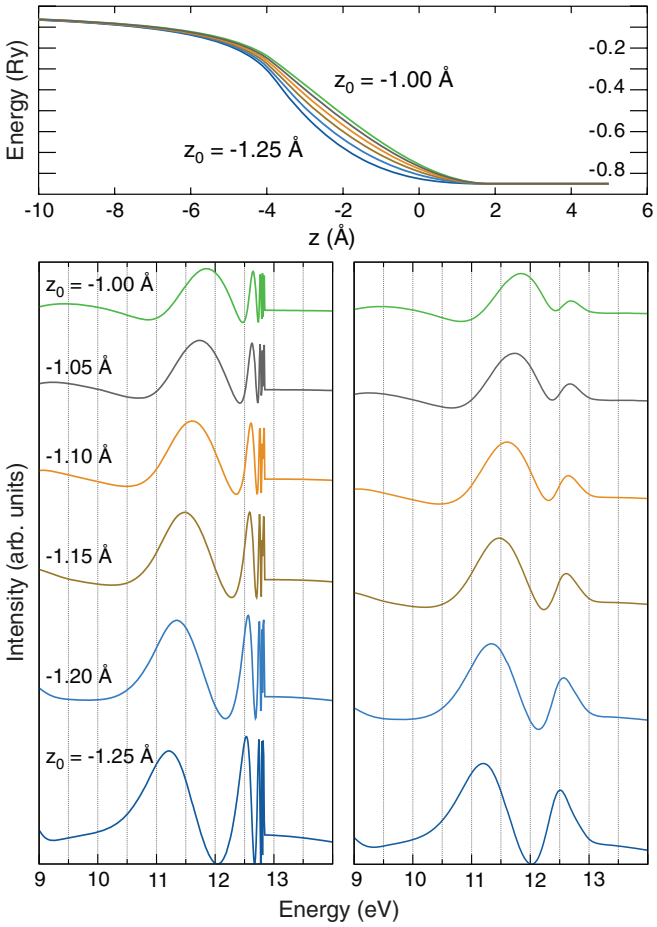

FIG. 8. (Color online) Calculated VLEED fine structures for different barrier shapes caused by different positions of the image plane (as shown in the top part). Left: Calculated fine structure. Right: Fine structure from left-hand side subject to an experimental resolution of $\Delta E = 150$ meV and $\Delta\varphi = 2.0^\circ$ and the corresponding equivalent resolution.

The influence of an experimental resolution of $\Delta\varphi = 2.0^\circ$ and $\Delta E = 150$ meV is shown on the right-hand side of Fig. 8. For the $\bar{1}\bar{1}$ fine structure of Cu(001) this resolution corresponds to a total equivalent resolution of 263 meV. The broadened spectra illustrate that differences in the maxima and minima

are still visible even if z_0 is changed by only 0.05 Å. The second peak visible in the spectra contains all higher-order peaks. Since the first peak position is most affected by changes in the barrier shape, the resulting peak shifts should be easily discernible in an experiment.

B. Spin-dependent barriers

For an evaluation of the feasibility of spin-polarized VLEED measurements, we have calculated the spin-dependent VLEED fine structures for the only spin-dependent barriers available in the literature. These barrier models were employed to successfully determine the energetic positions of the spin-dependent surface states on the Co(0001) (Ref. 34) and the Fe(110) (Refs. 30 and 31) surfaces.

Figure 9(a) presents the spin-dependent barrier for Co(0001) (Ref. 34) and the corresponding spin-dependent VLEED fine structure and spin asymmetry $(I^{\uparrow} - I^{\downarrow})/(I^{\uparrow} + I^{\downarrow})$ (calculated without experimental broadening). Strongly spin-dependent intensities as well as spin-dependent peak positions, especially of the first fine-structure peak, reflect the spin-dependent shape of the barrier.

For the case of the Fe(110) surface as shown in Figs. 9(b) and 9(c), the two surface barriers shown in the literature are not only quantitatively but qualitatively different. Nevertheless, both barriers were successfully used to describe the surface electronic structure of this particular surface. Both barriers show a similar behavior far away from the surface, where the spin dependence is reversed compared with Co(0001). Close to the crystal, however, the barrier published in Ref. 31 still has a deeper potential for minority-spin electrons, while the spin components of the barrier published in Ref. 30 cross at around -1 a.u. away from the surface. This results in remarkably different VLEED fine structures with distinct spin asymmetries. While the spin asymmetry in one case is positive for all energies of the fine structure, it changes sign repeatedly in the other case.

Note that the spin dependence in the Co and the Fe fine structure is of the same order of magnitude, while the absolute values of the spin asymmetry differ strongly. The latter is due to a large bulk-derived scattering background, on which this specific Fe fine structure appears.

Our calculation based on proven realistic barrier models clearly demonstrates the following:

(i) VLEED fine structures are sensitive enough to reveal detailed differences in the barrier shape in a study combining theory and measurement. The spin-dependent VLEED fine structures exhibit distinct differences, especially in the low-order members, that should be easily discernible in a spin-polarized VLEED experiment.

(ii) VLEED fine structures offer a much more versatile access to the surface barrier than the energetics of surface states. The latter depends on the existence of surface states and then provides information only for specific $E(k_{\parallel})$ values. VLEED, however, is capable of delivering a broad data set, because a scattering signal can be obtained as a function of energy and angles Θ and Φ continuously throughout large intervals.

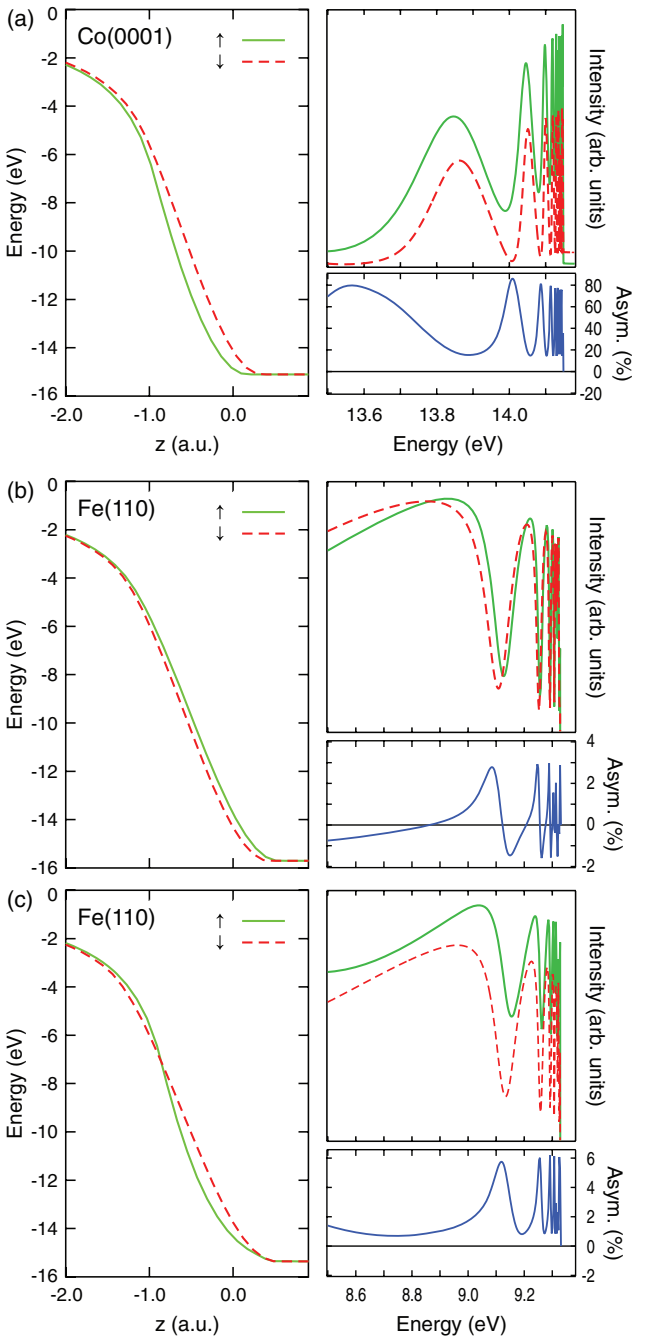

FIG. 9. (Color online) Top: Spin-dependent surface barrier (Ref. 34) (left) and resulting VLEED fine structure and spin asymmetry (right) for the Co(0001) surface. Shown here is the $\bar{1}0$ fine structure with incidence angles $\Theta = 30°$ and $\Phi = 0°$ along $\bar{\Gamma}\bar{M}$. The magnetization is also along $\bar{\Gamma}\bar{M}$. The majority-spin component is shown in green, the minority-spin component in red (dashed), and the spin asymmetry in blue. Middle: Spin-dependent surface barrier from Ref. 31 (left) and resulting VLEED fine structure and spin asymmetry (right) for the Fe(110) surface. Bottom: Spin-dependent surface barrier after Ref. 30 (left) and resulting VLEED fine structure and spin asymmetry (right) for the Fe(110) surface. The Fe $0\bar{1}$ fine structures shown here are calculated for $\Theta = 80°$ and $\Phi = 0°$ along $\bar{\Gamma}\bar{N}$. Magnetization is along the $\bar{\Gamma}\bar{N}$ direction as well. Note the qualitative difference in the spin dependence of the surface barriers and the correspondingly large differences visible especially in the first fine-structure peak.

The larger the data set, the more likely that a model potential which reproduces the complete experimental data set uniquely represents the true spin-dependent surface potential.

VII. CONCLUSION AND OUTLOOK

We have presented a feasibility study of how the shape of the spin-dependent surface barrier can be derived from spin-polarized VLEED fine-structure measurements. We started with a brief review of different surface-barrier models and described the origin of the VLEED fine structures. We discussed the requirements for experimental access to these fine structures. In this context, we emphasized the importance of the equivalent resolution. Finally, we presented realistic model calculations of spin-dependent fine structures for specific ferromagnetic surfaces. We come to the conclusion that spin-polarized VLEED experiments with state-of-the-art energy and angular resolution are able to reveal details of the spin-dependent shape of the surface barrier. Measurements of this kind are currently in progress with promising early results.

ACKNOWLEDGMENTS

The authors would like to thank S. Thurgate and R. Feder for helpful and stimulating discussions. One of the authors (J.B.) thanks H. Ebert for financial support through DFG (Grants No. FOR 1346, No. EB-154/18, No. EBE-154/23, and No. MI-1327/1) and BMBF (Grant No. 05K10WMA).

*markus.donath@uni-muenster.de

[1] E. McRae, Rev. Mod. Phys. **51**, 541 (1979).
[2] P. J. Jennings, R. O. Jones, and M. Weinert, Phys. Rev. B **37**, 6113 (1988).
[3] J. Rundgren and G. Malmström, J. Phys. C **10**, 4671 (1977).
[4] R. O. Jones, P. J. Jennings, and O. Jepsen, Phys. Rev. B **29**, 6474 (1984).
[5] S. M. Thurgate and C. Sun, Phys. Rev. B **51**, 2410 (1995).
[6] Y. A. Bychkov and E. I. Rashba, JETP Lett. **39**, 78 (1984).
[7] S. LaShell, B. A. McDougall, and E. Jensen, Phys. Rev. Lett. **77**, 3419 (1996).
[8] M. Hoesch, M. Muntwiler, V. N. Petrov, M. Hengsberger, L. Patthey, M. Shi, M. Falub, T. Greber, and J. Osterwalder, Phys. Rev. B **69**, 241401 (2004).
[9] L. Fu and C. L. Kane, Phys. Rev. B **76**, 045302 (2007).
[10] D. Hsieh, D. Qian, L. Wray, Y. Xia, Y. S. Hor, R. J. Cava, and M. Z. Hasan, Nature (London) **452**, 970 (2008).
[11] H.-J. Noh, H. Koh, S.-J. Oh, J.-H. Park, H.-D. Kim, J. D. Rameau, T. Valla, T. E. Kidd, P. D. Johnson, Y. Hu *et al.*, Europhys. Lett. **81**, 57006 (2008).
[12] Y. L. Chen, J. G. Analytis, J.-H. Chu, Z. K. Liu, S.-K. Mo, X. L. Qi, H. J. Zhang, D. H. Lu, X. Dai, Z. Fang *et al.*, Science **325**, 178 (2009).
[13] Y. Xia, D. Qian, D. Hsieh, L. Wray, A. Pal, H. Lin, A. Bansil, D. Grauer, Y. S. Hor, R. J. Cava *et al.*, Nat. Phys. **5**, 398 (2009).
[14] D. Hsieh, Y. Xia, D. Qian, L. Wray, J. H. Dil, F. Meier, J. Osterwalder, L. Patthey, J. G. Checkelsky, N. P. Ong *et al.*, Nature (London) **460**, 1101 (2009).
[15] H. Zhang, C.-X. Liu, X.-L. Qi, X. Dai, Z. Fang, and S.-C. Zhang, Nat. Phys. **5**, 438 (2009).
[16] E. G. McRae and C. W. Caldwell, Jr., Surf. Sci. **2**, 509 (1964).
[17] S. Andersson, Surf. Sci. **19**, 21 (1970).
[18] J. Lauzier, L. de Bersuder, and V. Hoffstein, Phys. Rev. Lett. **27**, 735 (1971).
[19] A. Adnot and J. D. Carette, Phys. Rev. Lett. **38**, 1084 (1977).
[20] E. G. McRae, D. Aberdam, R. Baudoing, and Y. Gauthier, Surf. Sci. **78**, 518 (1978).
[21] R. E. Dietz, E. G. McRae, and R. L. Campbell, Phys. Rev. Lett. **45**, 1280 (1980).
[22] G. Hitchen and S. Thurgate, Phys. Rev. B **38**, 8668 (1988).
[23] J. Kirschner and R. Feder, Phys. Rev. Lett. **42**, 1008 (1979).
[24] R. Feder, J. Phys. C **14**, 2049 (1981).
[25] D. H. Yu, C. Math, M. Meier, M. Escher, G. Rangelov, and M. Donath, Surf. Sci. **601**, 5803 (2007).
[26] D. T. Pierce, R. J. Celotta, G. C. Wang, and E. G. McRae, Solid State Commun. **39**, 1053 (1981).
[27] E. G. McRae, D. T. Pierce, G. C. Wang, and R. J. Celotta, Phys. Rev. B **24**, 4230 (1981).
[28] S. N. Samarin, J. F. Williams, A. D. Sergeant, O. M. Artamonov, H. Gollisch, and R. Feder, Phys. Rev. B **76**, 125402 (2007).
[29] F. Passek, M. Donath, K. Ertl, and V. Dose, Phys. Rev. Lett. **75**, 2746 (1995).
[30] M. Nekovee, S. Crampin, and J. E. Inglesfield, Phys. Rev. Lett. **70**, 3099 (1993); M. Nekovee and J. E. Inglesfield, Prog. Surf. Sci. **50**, 149 (1995).
[31] J. Braun, C. Math, A. Postnikov, and M. Donath, Phys. Rev. B **65**, 184412 (2002).
[32] A. Winkelmann, D. Hartung, H. Engelhard, C.-T. Chiang, and J. Kirschner, Rev. Sci. Instrum. **79**, 083303 (2008).
[33] T. Okuda, Y. Takeichi, Y. Maeda, A. Harasawa, I. Matsuda, T. Kinoshita, and A. Kakizaki, Rev. Sci. Instrum. **79**, 123117 (2008).
[34] C. Math, J. Braun, and M. Donath, Surf. Sci. **482–485**, 556 (2001).
[35] Unless explicitly stated otherwise, we employ atomic units, i.e. energy in rydbergs and distance in Bohr radii.
[36] P. Jennings and R. Jones, Adv. Phys. **37**, 341 (1988).
[37] N. D. Lang and W. Kohn, Phys. Rev. B **7**, 3541 (1973).
[38] G. Malmström and J. Rundgren, J. Phys. C **13**, L61 (1980).
[39] E. Tamura and R. Feder, Solid State Commun. **58**, 729 (1986).
[40] P. Jennings, Surf. Sci. **25**, 513 (1971).
[41] R. Jones and P. Jennings, Surf. Sci. Rep. **9**, 165 (1988).
[42] J. B. Pendry, *Low Energy Electron Diffraction* (Academic Press, New York, 1974).
[43] M. A. Van Hove and S. Y. Tong, *Surface Crystallography by LEED* (Springer, Berlin, 1979).
[44] G. Ertl and J. Küppers, *Low Energy Electrons and Surface Chemistry* (VCH, Weinheim, 1985).
[45] K. Heinz, Rep. Prog. Phys. **58**, 637 (1995).
[46] M. Escher, N. B. Weber, M. Merkel, L. Plucinski, and C. M. Schneider, e-J. Surf. Sci. Nanotech. **9**, 340 (2011).
[47] J. Le Bosse, J. Lopez, C. Gaubert, Y. Gauthier, and R. Baudoing, J. Phys. C **15**, 3425 (1982).

[48]P. M. Echenique and J. B. Pendry, J. Phys. C **11**, 2065 (1978).
[49]G. Gaubert, R. Baudoing, Y. Gauthier, J. C. L. Bosse, and J. Lopez, J. Phys. C **16**, 2625 (1983).
[50]C. Gaubert, R. Baudoing, Y. Gauthier, and J. Rundgren, Surf. Sci. **147**, 162 (1984).
[51]S. Thurgate and G. Hitchen, Appl. Surf. Sci. **24**, 202 (1985).
[52]G. Hitchen and S. Thurgate, Surf. Sci. **197**, 24 (1988).
[53]R. Feder and J. Kirschner, Surf. Sci. **103**, 75 (1981).
[54]H. Ebert *et al*., Computer code SPR-KKR, version 6.3, http://olymp.cup.uni-muenchen.de/ak/ebert/SPRKKR (2012).
[55]H. Ebert, D. Ködderitzsch, and J. Minár, Rep. Prog. Phys. **74**, 096501 (2011).
[56]M. Grass, J. Braun, G. Borstel, R. Schneider, H. Dürr, Th. Fauster, and V. Dose, J. Phys. Condens. Matter **5**, 599 (1993).